



## Development and Application of Hot Embossing in Polymer Processing: A Review

Jingyao Sun<sup>1</sup>, Jian Zhuang<sup>1</sup>, Ying Liu<sup>2</sup>, Hong Xu<sup>1</sup>, Jesse Horne<sup>3</sup>, Evan K. Wujcik<sup>3</sup>, Haichao Liu<sup>4</sup>, Jong E. Ryu<sup>5</sup>, Daming Wu<sup>1,2\*</sup> and Zhanhu Guo<sup>6</sup>

Hot embossing of polymer materials is a promising technology for the fabrication of high quality and precision patterns on the micro/nano-scales. There are three basic forms of hot embossing including, plate-to-plate (P2P), roll-to-plate (R2P), and roll-to-roll (R2R) hot embossing. It also can be divided into isothermal and non-isothermal hot embossing according to the different temperature control modes of polymer substrates and structured molds. This review reports recent progress made of hot embossing methods in polymer processing and the efforts to shorten its processing period for commercial applications. Research and innovations in simulation of hot embossing process and mold fabrication are also comprehensively summarized. Within this review, microfluidics, light guide plate (LGP), and other novel applications of hot embossing are systematically cataloged. Finally, challenges and future trends of hot embossing in polymer processing are presented and forecasted.

**Keywords:** Hot embossing; Micro-nano manufacturing; Processing period; Mold fabrication; Polymer-based devices

**Received** 21 October 2019, **Accepted** 8 December 2019

**DOI:** 10.30919/esmm5f605

### 1. Introduction

Micro/nano-manufacturing technology refers to a series of design, processing, and testing technologies for materials in the micro/nano-scale. Similar to biotechnology and information technology, it is one of the most desirable research fields and the most potential new developing market in the world in the 21<sup>st</sup> century.<sup>1-5</sup> Often, the manufacturing industry encourages researchers to develop high-precision processing technologies based on traditional processing methods. In order to meet the increasing demands of industry, the manufacturing level of precision has been gradually reduced from millimeter level ( $10^{-3}$  m) to micrometer level ( $10^{-6}$  m) and even on the order of nanometers ( $10^{-9}$  m). The concept of "micro/nano-manufacturing technology" emerged at this time.

Compared with inorganic materials such as glass and metal, polymer materials have higher thermal isolation, electrical isolation, and biocompatibility at a lower cost point.<sup>6-10</sup> The specific micro/nano-structures

of polymer surfaces also provide excellent tunability. Novel developments include superhydrophobic,<sup>11-14</sup> superhydrophilic,<sup>15-17</sup> antireflection,<sup>18-20</sup> light diffusion,<sup>21-23</sup> materials. Micro/nano-manufacturing technologies for polymer materials, include micro-injection molding,<sup>24-27</sup> micro-casting,<sup>28, 29</sup> electrospinning,<sup>30-32</sup> 3D printing,<sup>8, 33-35</sup> and hot micro/nano-embossing.<sup>36-40</sup> These have gradually become active research topics in recent years. Polymer materials are widely used in various research fields of different disciplines, such as chemistry, optics, bioengineering, and micro-electromechanical systems (MEMS); polymeric materials provide the numerous advantages of low cost, ease of large-scale processing, and a wide selection of chemical and physical properties. Some specific examples of polymer material applications include: diffraction module,<sup>41</sup> optical waveguide module,<sup>42, 43</sup> micro-lens array,<sup>44-46</sup> liquid crystal display,<sup>47, 48</sup> DNA sequencing and detector,<sup>49, 50</sup> polymerase chain reaction (PCR) amplification,<sup>51, 52</sup> biochips,<sup>53-55</sup> micro-fluidics,<sup>56-60</sup> micro-mixer,<sup>61, 62</sup> capillary electrophoresis,<sup>63</sup> etc.

Micro/nano-manufacturing technologies for polymer materials endow polymeric products with various unique functions by constructing different micro/nano-structure arrays on the surface of polymers. At present, extrusion micro-imprinting, injection molding, injection compression molding, and template embossing (including hot embossing and ultraviolet curing embossing) are the main processing methods for the fabrication of polymer micro/nano-structured devices.<sup>64-69</sup> Among the methods listed above, the first three methods are only suitable for the fabrication of micro-structured devices, while the template embossing technique presents a much better processing ability across the micro/nano-scales. Particularly, because of the simple apparatus requirement and processing technology, the hot embossing method can create precision forming at both the micro/nano-scales.<sup>70-73</sup> Due to such positive attributes, hot embossing has attracted much attention in recent years by both academia and industry.

The prototype of hot micro/nano-embossing technology first appeared in the 1970s. It was used by Radio Corporation of America

<sup>1</sup>College of Mechanical and Electrical Engineering, Beijing University of Chemical Technology, Beijing 100029, China

<sup>2</sup>State Key Laboratory of Organic-Inorganic Composites, Beijing, 100029, China

<sup>3</sup>Materials Engineering And Nanosensor [MEAN] Laboratory, Department of Chemical and Biological Engineering, The University of Alabama, Tuscaloosa, AL 35487

<sup>4</sup>Academic Division of Engineering, Qingdao University of Science & Technology, Qingdao 266061, China

<sup>5</sup>Department of Mechanical and Aerospace Engineering, North Carolina State University, Raleigh, NC 27695, USA

<sup>6</sup>Integrated Composites Laboratory (ICL), Department of Chemical & Biomolecular Engineering, University of Tennessee, Knoxville, TN 37996, USA

\*E-mail: wudaming@vip.163.com; zguo10@utk.edu

(RCA) to copy laser holograms in the playback device of a television video recording system. The laser holograms were successfully copied onto polyvinyl chloride insulating tapes.<sup>74</sup> Later, Ulrich and co-workers<sup>75</sup> successfully fabricated 7  $\mu\text{m}$  wide and 3.5  $\mu\text{m}$  deep structure arrays on polymethylmethacrylate (PMMA) substrates via a similar method using glass fibers as the embossing mold. In 1995, Chou *et al.*<sup>76</sup> at Princeton University achieved a major breakthrough in hot embossing technology: they successfully fabricated periodic nanogrooves with a width of 25 nm and a depth of 100 nm on the surface of a thermoplastic polymer substrate, which formally enabled the hot embossing technology to move from the micron-scale to the nano scale. The technological procedure of the hot embossing, as shown in Fig. 1,<sup>77</sup> comprises five steps: place the polymeric substrate into the mold, in-mold heating of the substrate under a press, holding the press to emboss, in-mold cooling of the embossed substrate, and finally demolding of the product. During the hot embossing process, the embossing mold needs to be heated to 10–40 °C above the glass transition temperature  $T_g$  (sometimes even higher than the melting temperature  $T_m$  or viscous flow temperature  $T_f$  of the material) and then be cooled to a temperature below  $T_g$  after certain time of holding the pressing force.<sup>78, 79</sup> Basically, thermoplastic polymers undergo two deformation stages in the whole hot embossing process: one is the strain hardening and stress concentration stage during the heating and embossing processes, and the other is the stress relaxation and deformation recovery stage during the cooling and demolding processes.<sup>80</sup> Glass transition temperature ( $T_g$ ), forming pressure and holding time are the most important parameters for hot micro/nano-embossing technology.

Many researchers around the world have systematically studied the relevant mechanism and technical apparatuses for the hot embossing method during the last two decades since its invention. Some enterprises in Germany, Japan, and the United States already have sold commercialized hot micro/nano-embossing apparatus. Besides being used as an experimental apparatus, these commercialized hot micro/nano-embossing setups have also been used in the fabrication of microfluidics, micro-optical devices, and other micro/nano-structural

products.<sup>81, 82</sup>

## 2. Classification of Hot Embossing Methods

As one of the most potential micro/nano systems that can be widely applied in the near future, polymer micro/nano systems and their manufacturing technology play extremely important roles in the field of micro/nano manufacturing. In this section, we will first make a brief comparison among several commonly used polymer micro/nano manufacturing technologies, and then systematically elaborate the classification on hot micro/nano-embossing methods.

### 2.1 A Brief Comparison Among Commonly Used Polymer Micro/Nano Manufacturing Technologies

Micro-injection molding, micro-extrusion technology, and template embossing (also known as “micro/nano-imprinting lithography”) are the three main kinds of micro/nano-manufacturing technologies for polymer materials. Among them, template embossing methods can be further divided into hot embossing and ultraviolet curing embossing.<sup>83–87</sup> The processing temperature ranges and the advantages and disadvantages of the aforementioned methods are listed in Table 1.

The method of micro-injection molding has become one of the most commonly used processing methods for polymer materials in industry due to its advantages of having a low cost, high efficiency, and good adaptability of product size and geometry.<sup>88–93</sup> The world's first specialized micro-injection molding apparatus was developed in Germany in 1985. After that, various kinds of micro-injection molding apparatuses were subsequently developed in other countries, which provided strong support for the international development of the micro-injection molding technology. The explosive development of micro injection molding apparatuses also effectively guaranteed the translation to mass production of polymeric products on the micro-scale.

Micro-injection molding apparatuses can be divided into three categories according to their different plasticizing and injection molding units.<sup>94–96</sup> (1) Plunger-type: There are two kinds of plunger type injection molding apparatuses: single plunger-type and double plunger-type. The

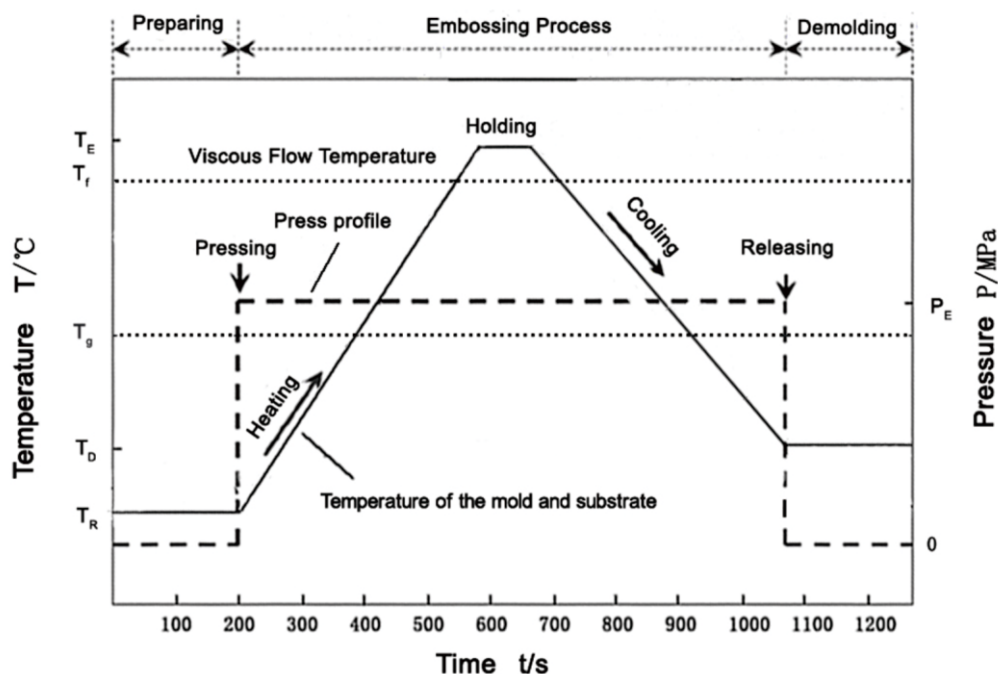


**Fig. 1** Procedures diagram of the traditional hot embossing process ( $T_R$  – Room Temperature;  $T_E$  – Embossing Temperature;  $T_D$  – Demolding Temperature;  $P_E$  – Embossing Pressure).

melted polymer materials in single plunger-type apparatus are driven by the plunger and enter the mold cavity from the nozzle through the torpedo spreader for better plasticization. For double plunger-type apparatuses, the plasticization and quantity measurement are performed separately by two groups of plungers. (2) Screw-type. The plasticizing, measuring and injection molding functions in screw-type apparatuses are all performed by the screw. The action of a linear motion mechanism and the rotation of internal components in screw-type apparatuses are all completed on the same central axis, which provides the advantages of simple structure and easy control. (3) Plunger-screw hybrid type. In the plunger-screw hybrid type apparatus, the plasticization and blending of polymer materials are performed by the screw, while the precise measurement and injection molding of the polymer melt is performed by the plunger mechanism, which is controlled by a servo motor. The structure of the plunger-screw hybrid type apparatus is complex, and apparatus maintenance is difficult. However, the processing and control accuracy is higher than those of plunger type and screw type apparatuses.

Micro-extrusion could realize the continuous fabrication of polymeric products with the same cross-section. Thus, micro-extrusion technology is widely applied for the fabrication of micro-optical fibers, micro-gears, micro-catheters, and other high precision devices.<sup>97-99</sup> Researchers around the world have produced a great amount of work on the flow behavior of polymer materials on the micro-scale, including the flow of polymer melts in micro-channels,<sup>100, 101</sup> the optimal designation of extruder die,<sup>102, 103</sup> the effect of surface tension of polymer melt on micro extrusion forming,<sup>104, 105</sup> and the wall slip phenomenon in polymer micro extrusion.<sup>106</sup> The aforementioned research works have laid the groundwork of a theoretical foundation for the further development of micro-extrusion technology.

The template embossing methods can be further divided into hot embossing and ultraviolet curing embossing. The three different forming principles of both hot embossing and ultraviolet curing embossing can be distinguished by the configuration of the molds: plate-to-plate (P2P),<sup>107, 108</sup> roll-to-plate (R2P),<sup>109, 110</sup> and roll-to-roll (R2R).<sup>111-114</sup> In hot embossing processes, polymer substrates will be heated to a temperature

higher than their glass transition temperature ( $T_g$ ) or melting temperature ( $T_m$ ), and then apply appropriate pressure to form the structure transfer from mold to polymer substrates. Compared with the method of micro-injection molding, there is much less temperature change in the polymer material during the hot embossing process. Therefore, the contraction rate of products fabricated by the hot embossing method is smaller, which thus leads to higher shape and dimensional precision. However, the traditional hot embossing method has a fatal flaw in processing efficiency and makes it unsuitable for mass industrial production. At present, the hot embossing method is mainly used in the laboratory for the small batch production of prototype products. We also discuss current technologies for cycle time reduction reported by researchers globally in the following sections.

The ultraviolet curing embossing technology was first proposed by Grant Wilson of Texas State University in 1999.<sup>115</sup> Ultraviolet curing embossing uses photosensitive polymers as the embossing material. Only a minute pressure is needed during the ultraviolet curing embossing process to promote the transformation of the ultraviolet curable polymer into micro/nano-structured mold cavities. The ultraviolet light source is used for irradiation curing at the same time to solidify and obtain micro/nano-structured products. Fig. 2 shows the schematic diagram of the R2P ultraviolet curing embossing technology. There are no heating and cooling steps involved in the ultraviolet curing embossing process, so the influence of thermal deformations of the mold and polymer materials on the forming accuracy of final products is negligible. However, the application of the ultraviolet curing embossing method is strongly limited by the inherent disadvantages of having a high cost for the raw materials and the apparatus and the poor mechanical properties of final products.

## 2.2 The Classification of Hot Micro/Nano-Embossing Methods

As mentioned previously, the hot micro/nano-embossing methods can be distinguished into three different types according to the configuration of molds: plate-to-plate (P2P), roll-to-plate (R2P) and roll-to-roll (R2R). Fig. 3a shows the schematic diagram of the P2P hot embossing method, which is the conventional method of the hot embossing process that is

**Table 1** A brief comparison of several polymer micro/nano manufacturing technologies.

Processing method	Temperature window	Advantages	Disadvantages
Micro injection molding	$> T_m(T_f)$	High efficiency; High precision;	Limited product thickness; High processing pressure;
Micro extrusion	$> T_m(T_f)$	High efficiency; Continuous manufacturing;	Low precision; Not suitable for the fabrication of nanostructures;
Hot embossing	$T_g + \Delta T \sim T_m(T_f)$	High precision; Low cost for apparatus; Trans - micro/nano scale manufacturing;	Low efficiency (especially for traditional hot embossing method);
Ultraviolet curing embossing	Room Temperature	High precision; No heating required; Trans - micro/nano scale manufacturing;	High cost for raw materials and apparatus; Poor mechanical properties of products;

most commonly implemented for industrial applications. It can be seen that the P2P hot embossing contains a flat structured mold and a flat basal substrate. Although P2P hot embossing has the advantages of easy operation, a simple apparatus, and high accuracy, it is a stepwise discontinuous method with limited processing efficiency and forming area. In order to meet the increasing demands for large-area structure replication, two different kinds of R2P hot embossing methods are proposed by researchers. One kind consists of a roller-structured mold and a flat basal substrate (as shown in Fig. 3b), while another consists of a pressure roller, a flat-structured mold, and a flat basal substrate (as shown in Fig. 3c). The continuous replication of micro/nano-structures via the hot embossing method becomes possible after switching from the P2P method to the R2P mode. However, only the R2R hot

embossing method is a truly continuous fabrication method with high efficiency and high accuracy, when compared with the R2P hot embossing. As shown in Fig. 3d, the R2R hot embossing system contains two rollers: one is the structured mold, and the other is the basal substrate. In some special cases, the basal substrates introduced above for P2P, R2P, and the R2R hot embossing methods will also be patterned to have a one-step fabrication of polymeric products with double-sided structures.

The hot embossing technology has achieved rapid development during the last 50 years since its appearance in the 1970s. The study on apparatus design and development started early internationally, and most of the hot embossing apparatuses were designed and developed by scientific research institutes, including the Ohio State University (USA),

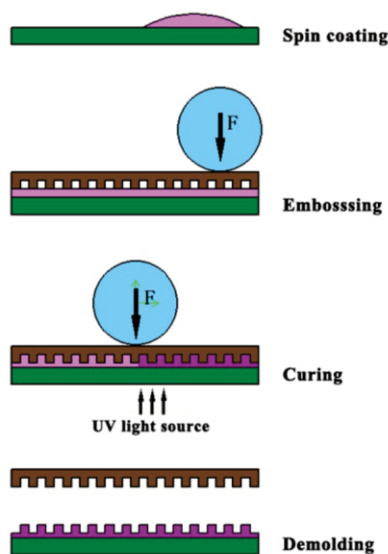


**Fig. 2** A schematic diagram of R2P ultraviolet curing embossing technology.

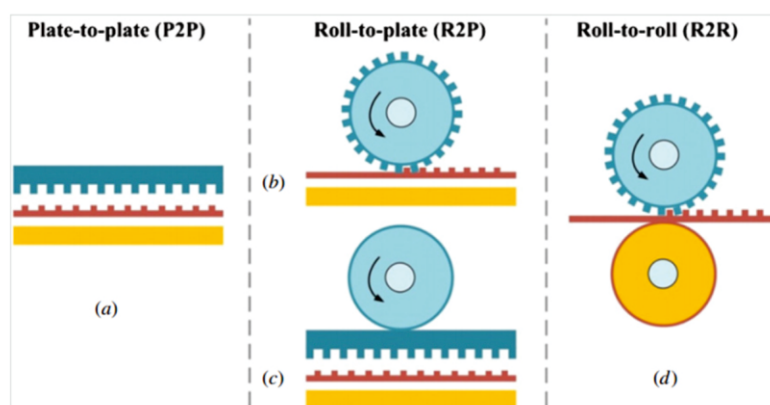


**Fig. 3** Schematic diagrams of (a) P2P hot embossing, (b) R2P hot embossing with roller mold, (c) R2P hot embossing with flat mold, and (d) R2R hot embossing (Reproduced with permission<sup>36</sup>).

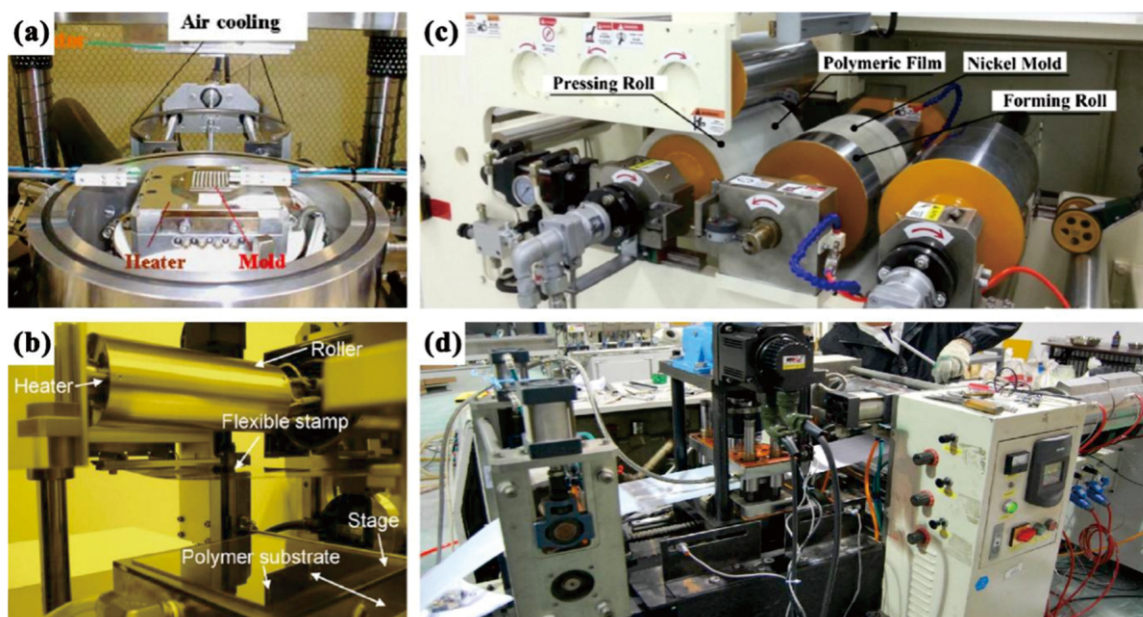


**Fig. 4** (a) A typical P2P hot embossing apparatus (Reproduced with permission<sup>116</sup>); (b) An overview of the R2P hot embossing apparatus (Reproduced with permission<sup>117</sup>); (c) The experimental R2R hot embossing apparatus (Reproduced with permission<sup>118</sup>); and (d) Our self-designed P2P apparatus in Beijing University of Chemical Technology.

Pohang University of Science and Technology (Korea), Karlsruhe Institute of Technology (Germany), among many other institutions. Typically, the performance of the initial prototype apparatus is relatively poor, with limited temperature and pressure control accuracy. With the rapid development of micro/nano-manufacturing technologies and the in-depth study on hot embossing process, researchers around the world found that the main processing parameters of hot embossing were mold temperature, pressure, embossing time, and the vacuum environment. Meanwhile, the research and development of the hot embossing apparatus trended towards high precision, accurate control, and high performance. Although the domestic research on the hot embossing apparatus is rather backward compared with foreign countries, the achievements in this field are remarkable. Many research institutes, including the Huazhong University of Science and Technology, Dalian University of Technology, Zhejiang University, Beijing University of Chemical Technology, among many others, have developed their own characteristic hot embossing techniques.

Fig. 4a presents a typical P2P hot embossing apparatus developed by Shan and coworkers from the Singapore Institute of Manufacturing Technology (Singapore).<sup>116</sup> It contains alignment mechanisms, top and bottom heaters, a vacuum chamber, and an air-cooling system using circular pipes with air-nozzles. The highest mold temperature that can be reached is 350 °C and has a maximum loading capacity of 25 kN for this hot embossing process. Youn *et al.*<sup>117</sup> from National Institute of Advanced Industrial Science and Technology (Japan) proposed a prototype of an R2P hot embossing apparatus (as shown in Fig. 4b). This R2P system is made up of a press force and moving speed control system, a one-axis moving platform, a roller embossing system with a pressure control component, and a computer for processing parameters input and experimental data acquisition. This R2P hot embossing apparatus can provide up to a 2 kN maximum tangential force, with a relatively high precision of micro-Newtons. Lai's group<sup>118</sup> from Shanghai Jiao Tong University (China) designed and developed an experimental R2R hot embossing setup for continuous fabrication (as shown in Fig. 4c). The forming system contains two rollers, a forming roller and a pressing roller. The forming roller is the actively driving roller with a heating component inside, while the pressure roller is the passive driving roller for force provided during the hot embossing process. The size of two rollers is 250 mm in diameter × 300 mm in length, the roller feeding speed is controllable in the range of 0.1 to 10 m/min, the temperature range of the forming roller is 25 to 300 °C, and the

maximum press force provides by the pressing roller is 500 N. Besides the hot embossing apparatuses introduced above, our group also had designed and developed an apparatus for P2P hot embossing.<sup>119, 120</sup> As shown in Fig. 4d, an extrusion machine was placed in front of the hot embossing system to provide a flat polymer substrate for semi-continuous step-by-step fabrication. The maximum press force during hot embossing process was 50 kN with a control accuracy of ±50 N, while the mold temperature was adjustable in the range of room temperature to 170 °C with a control accuracy of ±1 °C. The moving speed of the upper mold was controlled by a servo motor and could be set from 0.5 to 5.0 m/s. The effective area of our self-designed P2P hot embossing apparatus was 160 mm×80 mm, and a PLC control system was used to achieve accurate and intelligent control of the whole P2P hot embossing process.

### 3. Efforts to Shorten the Processing Period of Hot Embossing

An inherent problem of the long cycle time of conventional hot micro-embossing is mainly ascribed to periodically heating and cooling of the embossing mold with high thermal inertia. The whole cycle time of hot embossing used to be more than 10 minutes. Due to its long cycle time, the hot embossing method did not show competitiveness in mass production in cost and efficiency when compared with other common processing methods like micro-injection molding. In order to cut down the cycle time of the hot embossing method, researchers around the world have made great efforts on process optimization and device improvement in recent years. Although these efforts have led to significant progress in different aspects, there are still challenges in bringing hot embossing to the commercial scale.

The most typical way to reduce the cycle time of hot embossing was by making the heating and cooling process much faster. T. E. Kimerling and Donggang Yao<sup>121</sup> investigated a unique structured embossing tool with a rapid heating and cooling capability. Different miniaturized features, including micro-square and hexagonal wells, micro-circular holes, and submicron surface features were successfully fabricated with a total embossing cycle time around 20 s. The authors declared that their technology was reliable and durable for the replication of microscale features. Fig. 5a shows the experimental setup for their rapid thermal response (RTR) hot embossing system. They modified an Instron universal testing machine to be a press for

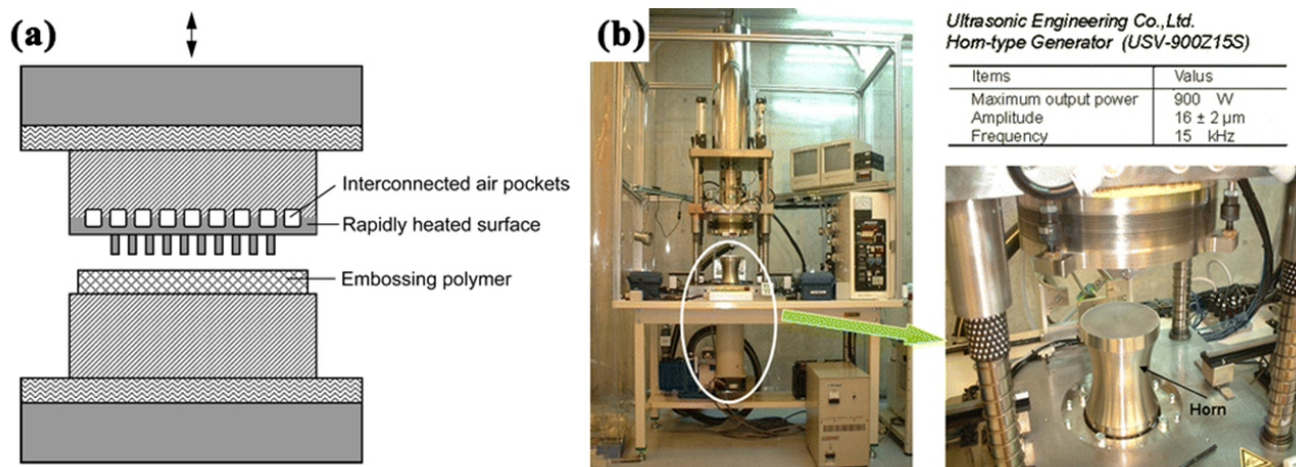


Fig. 5 (a) Schematic of the experimental setup of rapid thermal response hot embossing (Reproduced with permission<sup>122</sup>), and (b) Photograph of the ultrasonic-vibration hot embossing device (Reproduced with permission<sup>123</sup>).

embossing. A mold with low thermal inertia was mounted to the end of the compression part to allow for the rapid heating and cooling capability. The polymer substrates were fixed using a vacuum fixture during the hot embossing process, and compressed air was supplied for mold cooling before demolding. Mekaru *et al.* studied the feasibility of ultrasonic heating and obtained good replication with a heating and cooling time as short as 60 seconds.<sup>122</sup> It was found that ultrasonic heating could form a melting layer on the polymer surface in several seconds while the temperature of the inner layer remained low. As shown in Fig. 5b, they installed a longitudinal ultrasonic vibration generator (frequency 15 kHz, vibration width  $16 \pm 2 \mu\text{m}$ , output 900 W) into a vacuum hot embossing device to provide ultrasonic vibration during the hot embossing process. Liu and co-workers proposed an infrared hot embossing process, and polymeric micro-block arrays with a dimension of  $100 \mu\text{m} \times 80 \mu\text{m} \times 40 \mu\text{m}$  were successfully fabricated in a shorter cycle time.<sup>123</sup> Pengcheng Xie and James Lee presented a rapid hot micro-embossing technique utilizing micro-patterned silicon stampers with a carbide-bonded graphene coating layer of about 45 nm thick to implement rapid heating and cooling. Their cycle time was shorter than 25 s.<sup>124</sup>

Many efforts have also been made to optimize the parameters and devices of the hot embossing process. Worgull *et al.* performed a series of experiments to meet the requirements increasing embossing surface area and simultaneously decreasing structure size.<sup>78</sup> Optimization of the hot embossing process was also researched by He *et al.*, and a well-replicated micro rectangular structure with high aspect ratio of 4 was obtained.<sup>125</sup> They further built a simplified hot embossing machine, and the best imprint quality for micro linear arrays on PMMA was achieved with a mold temperature of  $150^\circ\text{C}$ .<sup>126</sup> Wiryakun *et al.* presented a two-step hot embossing method to produce cross-shape microchannels with mold temperatures of  $180^\circ\text{C}$  and  $125^\circ\text{C}$ .<sup>127</sup> All these studies present great progress made in the field of the hot embossing method in recent years, but there were still some challenges to be resolved.

It was found that more than 90% of the cycle time was consumed for heating and cooling the mold and the polymeric substrate in conventional hot embossing processes. To achieve free heating and cooling of the embossing mold, a new method called isothermal hot embossing in the solid-like state (IHES) was proposed in 2016 by our group to cut down on the cycle time.<sup>119, 120</sup> Solid-like state, quite different from a highly elastic state, is a state that deformation can happen and completely maintain only when the material is under appropriate processing conditions. It should be pointed out that the "isothermal" in

IHES had a quite different meaning from what people called "isothermal hot embossing" before. The "isothermal" in traditional isothermal hot embossing meant that the mold and polymer substrate were heated and cooled together, while the "isothermal" in IHES represents that the mold temperature was kept constant at the setting value and was irrelevant to the exact situation of the polymer substrate. PMMA and polypropylene (PP) substrates were chosen as representative materials for amorphous and crystalline polymers to validate the feasibility of IHES. The main difference observed with IHES with traditional hot embossing was in their thermal pattern, such that the temperature of the molds for IHES was maintained at the setting value in the whole embossing cycle, no heating or cooling of the molds was needed as in traditional hot embossing process. In this way the cycle time of IHES could be reduced to 20–60 seconds, only 1/30 of the traditional hot embossing process.

For amorphous polymers like PMMA, the IHES method could be divided into two types according to the differences in initial mold temperature. As shown in Fig. 6a, in the IHES process, the PMMA substrate could be directly placed in the embossing mold without pre-heating if the mold temperature was set at a value above  $T_g$ . Pre-heating of the substrate was needed only when the temperature of the embossing mold was set at a value below  $T_g$ , as shown in Fig. 6b, that the substrate ought to be heated to a temperature above its  $T_g$  before it was placed in the embossing mold. It was available to press the substrate once it was placed in the mold, and the cooling of the substrate underwent together with the pressing process because the temperature of the mold was set near  $T_g$ . The most important parameter of the IHES process was the mold temperature, which should be reasonably determined to ensure sufficient deformation ability of the substrate before the cavity filling process finished. It is also essential to take the stress relaxation behavior of the substrate in embossing process into consideration while determining the mold temperature and holding duration for the IHES process.

In the IHES process, the molding window was designed in the area of around  $T_g$ . It is needed to state that the molding window refers to the temperature of the embossing mold, rather than the temperature of the substrate, and the pre-heated temperature of the substrate should be, in principle, above  $T_g$  for pre-heated type (Fig. 6b). In the period of embossing, the temperature of the substrate decreased from pre-heated temperature to the temperature of embossing mold,  $-5^\circ\text{C}$  to  $+10^\circ\text{C}$  around  $T_g$ , which was pre-calculated or optimized by experiment according to the characteristic of the polymer and the geometry of the

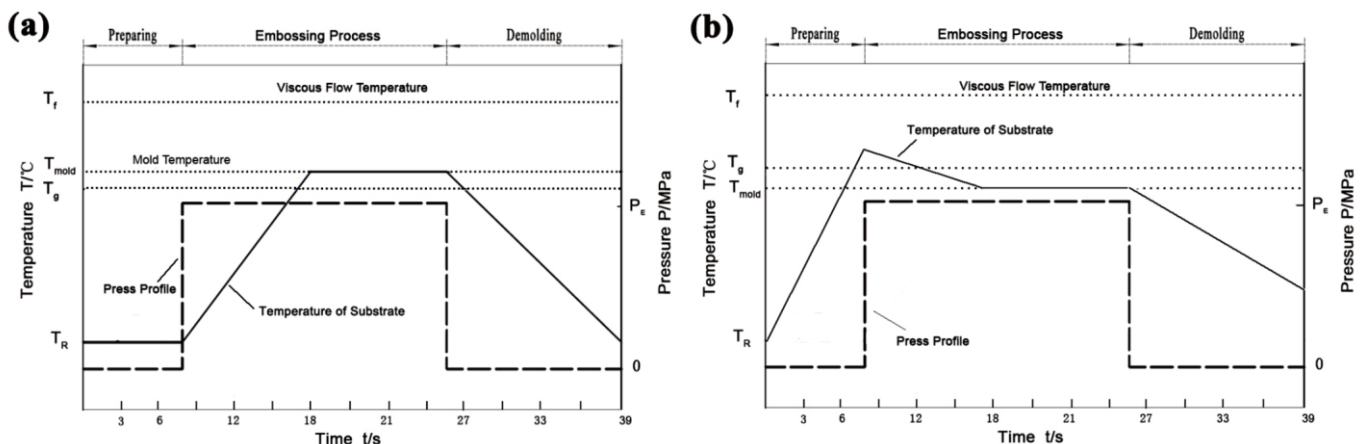


**Fig. 6** Two different procedure diagrams of the IHES process for amorphous polymers with mold temperature (a) higher, and (b) lower than  $T_g$  ( $T_R$  – Room temperature;  $T_{mold}$  – Mold temperature;  $P_E$  – Embossing pressure).

targeting micro/nano-structure.

For crystalline polymers like PP, the IHESS process is slightly different from that for the amorphous polymers introduced above. The region above  $T_g$  and below  $T_m$  was chosen as the molding window of IHESS method for crystalline polymers (as shown in Fig. 7). Two fundamental factors should be taken into consideration in estimating the press and thermal pattern of the IHESS process. Firstly, sufficient stress beyond the yield limit of PP should be applied to the substrates inducing forced high elastic deformation to fill in the mold cavities. Secondly, the thermal pattern should ensure that a majority of the inner stress induced by the embossing process could be relaxed before the demolding of the embossed product and that no detectable changes in shape and dimension of the embossed micro-structures can be demonstrated as a result of creep. With the goal of high replication, the mold temperature should be chosen as low as possible, as lower temperature of the demolding product had a relatively low speed of creep and easy to be cooled to ambient temperature. But too low of a mold temperature results in very high pressures and high residual stress in products. Based on an overall consideration of above factors, the mold temperature could range from 105 °C to 125 °C for PP.

Yao *et al.*<sup>128</sup> introduced another kind of “constant-temperature embossing” method in 2014. Slowly crystallizing polymers such as polyethylene terephthalate (PET) and polyether ether ketone (PEEK) were quenched during melt processing to produce amorphous films, and then reheated and embossed appropriately above  $T_g$  under constant mold temperature. In the way of phase transition, directly demolding with few defects was available at a single temperature. The phase transition process was unnecessary in the IHESS process compared with Yao's method, so amorphous polymers, like PMMA, can be used to produce transparent optical devices. Several strategies can be performed to avoid the stickiness during demolding of the IHESS without in-mold solidification process. In the case of PMMA, the mold temperature should be set to a narrow range around  $T_g$  to ensure a high modulus. Setting different temperatures around  $T_g$  of the upper and bottom molds, which is a future research project called “thermal differential embossing,” can ease the tackiness to a large extent. A surface treatment for the embossing mold will also help to reduce the risk of product sticking.

#### 4. Macroscopic and Microscopic Simulations of Hot Embossing

Researchers around the world have performed a lot of experimental

studies on the influences of processing parameters, including the materials of the mold and polymer,<sup>129-133</sup> mold temperature, pressure, holding time, and structure type<sup>134</sup> on the forming results of final products (e.g. duplication rate, uniformity, etc.). These tests for various kinds of polymer materials have provided useful information for parameter optimization, apparatus design, and method improvements of the hot embossing technology. Moreover, the influences of factors, such as stress relaxation and creep on the flow and deformation behavior of the polymer substrate, were systematically investigated through experimental methods.<sup>135,136</sup> Different kinds of mold materials with low surface energy and anti-sticking layers were also researched to reduce the defects caused by the adhesive force between the molds and the polymer substrates. However, these experiments could only provide information after embossing, which means the information and phenomena during the hot embossing process are hidden from researchers. In other words, experimental studies have restrictions on parameter optimization and method improvement because it is a black-box process. In order to examine and understand the various phenomena, such as the deformation behavior of the polymer substrate and the adhesion and damage of obtained structures, occurring in the hot embossing process, researchers have had to develop suitable analytical methods for systematic analysis. Researchers can examine the specific influences of processing parameters on the hot embossing process using analytical methods.

Numerical simulation is one of the most commonly used methods among analytical techniques. Numerical simulation methods could be further divided into macroscopic and microscopic simulations according to the different dimension scales of the research objects. The finite element method (FEM) is the primary method for macroscopic simulation.<sup>137-140</sup> To avoid possible distortions and misunderstandings caused by limited information, simulations of the whole hot embossing process (especially the embossing and the demolding steps) are needed. However, although the simulation of the embossing step is relatively perfect in the macroscopic world (e.g. FEM simulation for injection molding), the simulation method for the demolding step is quite inadequate. Thus, the macroscopic simulation for the whole hot embossing process was split up into two sub-processes, as there is no macroscopic software available for the description of the whole process. In other words, the macroscopic simulations for the embossing and demolding steps of hot embossing should be performed individually.

For the macroscopic simulations of the embossing step, the simulation software MOLDFLOW and DEFORM were applied using

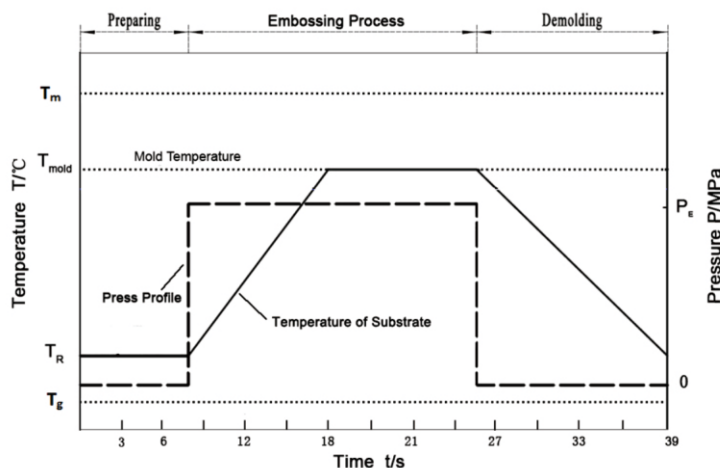


Fig. 7 Procedure diagram of the IHESS process for crystalline polymers.

similar features and settings as injection compression molding. MOLDFLOW was more suitable for higher mold temperatures (e.g. around  $T_m$  of crystalline polymers, around  $T_f$  or much higher than  $T_g$  of amorphous polymers), while DEFORM was more applicable to simulations at lower temperatures (e.g. around or a little higher than  $T_g$  of amorphous polymers). Qualitative results, including filling process of mold cavities, flow behavior of polymer melt, thickness variation of residual layer, and pressure distribution in polymer substrate, etc., could be obtained using aforementioned simulation software. For the macroscopic simulations of the demolding step, another commercial FEM simulation software named ANSYS was widely applied. The structural damages can be predicted using this software. Meanwhile, the processing parameters during the demolding step can also be optimized to reduce the possible damages caused by the demolding force.<sup>80, 141-147</sup>

The simulation methodology of macroscopic simulations can be summarized as follows:

First, create a mold and impose constraints on the boundaries. Fig. 8a shows the commonly used single-cavity two-dimensional FEM model with boundary conditions.<sup>148</sup> Normally, the interface between the mold and polymer substrate was defined as glued to avoid the displacement and stress discontinuity across the interface. The application of a symmetric boundary condition on the left and right sides, zero vertical displacement and adiabatic thermal boundary condition on the bottom, and the mold on the top make up a closed cavity together. Second, set the material properties (e.g. Young's modulus, Poisson's ratio, thermal expansion coefficient, density, flow stress data for the polymer, etc.), and use the governing equations (e.g. Navier–Stokes equation, mass conservation equation, force equilibrium equation, strain rate-velocity relation, mechanical constitutive relation, etc.) to meet the specific simulation requirements. After that, several process assumptions should be made to simplify the simulation. For example, (1) the inertial force, gravity, and friction are ignored; (2) there

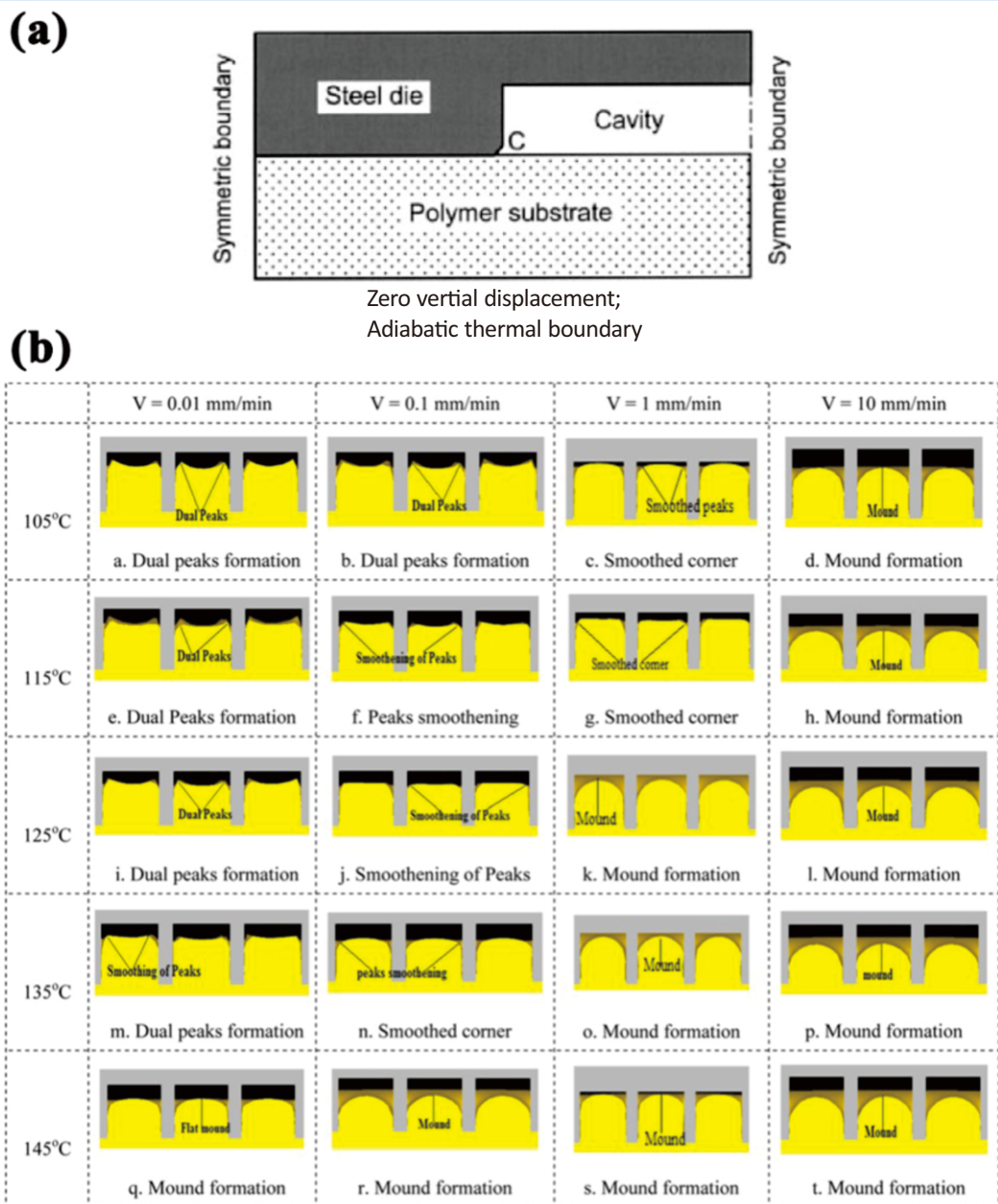


Fig. 8 (a) Single-cavity two-dimensional FEM model (Reproduced with permission<sup>148</sup>), and (b) the simulation result of hot embossing (Reproduced with permission<sup>149</sup>).

is no initial stress in the polymer substrate at the molding temperature; (3) the flow stress of the polymer is much less than shear stress and thermal stress at the interface between the mold and polymer; (4) the properties of the mold and polymer are all isotropic; (5) sliding is allowed (or ignored) at the interface between the mold and polymer, among others. Then, the simulation process can begin after the whole model is meshed and layout properly. Joshi *et al.*<sup>149</sup> performed a series of simulations using DEFORM to analyze the single and dual peak formation mechanism of the hot embossing method under varying processing parameters (e.g. mold temperature, molding velocity, etc.). Based on the simulation results presented in Fig. 8b, researchers showed that the proper mold temperature for PMMA in hot embossing should be 20–30 °C higher than its glass transition temperature, while the proper molding velocity should be in the range of 0.01–0.1 mm/min.

It is worth noting that the FEM model presented in Fig. 8a is a single-cavity model. The influence of neighboring cavities on deformation behavior is ignored in this simplified model. However, the hot embossing process is a deformation process of a polymer in non-closed cavities. The simplified model with the closed cavity will obviously increase the forced deformation and internal stress of the polymer, which leads to a definite error in real situations. In order to solve the inherent problem of a closed single-cavity model, we considered the influence of neighboring cavities and defined open boundary conditions to establish a non-closed multi-cavity model (as shown in Fig. 9). Uniform pressure is applied to the mold and the polymer substrate during simulation analysis, and the simulated results of the mid-cavity are chosen to be the final results.<sup>37</sup>

Although the macroscopic simulations mentioned above could provide useful information about the deformation behavior of the polymer during the hot embossing process, there are still many limitations. For example, the FEM method cannot predict the deformation behavior of the polymer when the target structure is smaller than hundreds and even tens of nanometers. This is due to the properties of the polymer behaving differently on the nano-scale. Moreover, the interaction between the atoms of the mold and the molecule chains of the polymer on the nano-scale can not be included in the macroscopic simulations using the FEM method. As a widely used microscopic simulation method, the molecular dynamics (MD) simulation is expected to have advantages over FEM method for systematic analysis of the hot embossing method on the nano-scale.<sup>150–155</sup>

The methodology of MD simulations is summarized as follows:<sup>156, 157</sup>

First, build a lattice model of the hot embossing system. The model of the polymer and mold should be built separately, and then adjust the cell parameters of the polymer layer to reach the mold layer for further integration. Perform energy minimization calculations on the polymer monomer to obtain the optimum structural properties of the polymer layer. The degree of polymerization, the total number of monomers in the polymer chain, the density of the polymer layer, and

other parameters should be determined in this step. The setting of a vacuum layer at a certain distance above the embossing system is also needed to avoid the influence of three-dimensional periodic boundary conditions on height. Secondly, set the boundary conditions of the simulated region (periodic boundary or nonperiodic boundary), and select the potential functions of interatomic interaction. The COMPASS force field is applied for the stress calculation, and the van der Waals force is calculated by the Lennard-Jones function. The potential energy expressions for translation, rotation, and torsion of the polymer chains are listed below.

$$\Phi_{bond} = \frac{1}{2} K_{bond} (l_{ij} - l_0)^2 \quad (1)$$

$$\Phi_{angle} = \frac{1}{2} K_{angle} (\theta_{ijk} - \theta_0)^2 \quad (2)$$

$$\Phi_{torsion} = \sum_{m=0}^3 a_m \{\cos(\theta_{ijkl})\}^m \quad (3)$$

where  $\Phi_{bond}$ ,  $\Phi_{angle}$ , and  $\Phi_{torsion}$  are the potential energy expressions for translation, rotation, and torsion of the polymer chains,  $l_{ij}$  is the bond length,  $l_0$  is the equilibrium bond length,  $K_{bond}$ ,  $K_{angle}$ , and  $a_m$  are energy constants,  $\theta_{ijk}$ ,  $\theta_0$ , and  $\theta_{ijkl}$  are the bending angle, equilibrium bending angle, and twist angle, respectively.

After that, set the initial position and initial velocity of all the particles in the hot embossing system. The equations of motion should be discretized by a specific algorithm, such as the Verlet algorithm, the leap-frog algorithm, the Beeman algorithm, and so on. Then the simulation results would be obtained after the system reaches an equilibrium state.

MD simulations of hot embossing processes using male and female molds were performed separately by Kim's group and Lee's group.<sup>151–153, 158</sup> Kim *et al.*<sup>153</sup> reported a hot embossing process using a male quartz mold, PMMA film, and a nickel floor substrate (as shown in Fig. 10a). The deformation behavior, density distribution, and stress distribution of the polymer film were researched using two molds with different aspect ratios. The springback phenomenon of the polymer residual layer was only observed during the hot embossing process using a high aspect ratio mold because the residual stress in the polymer film was much stronger in this scenario. Lee and co-workers<sup>158</sup> investigated the hot embossing process using a female nickel mold, amorphous polyethylene (PE) film, and silicon floor substrate (as shown in Fig. 10b). They found that the free volume reduction in the polymer film was the main reason for the density difference between the top and bottom regions. They further concluded that the formation of nanostructures in the hot embossing process depended more on the molecular compression than the bulk flow of the molecule chains.

## 5. Mold Fabrication

Micro/nano-structured molds are one of the most important components in the hot embossing process. High-quality molds with excellent

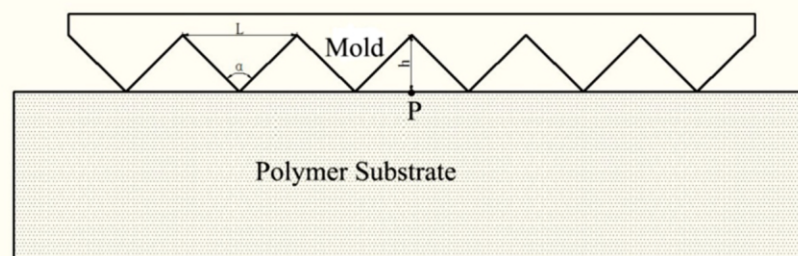


Fig. 9 Non-closed multi-cavity model for macroscopic simulation of hot embossing.

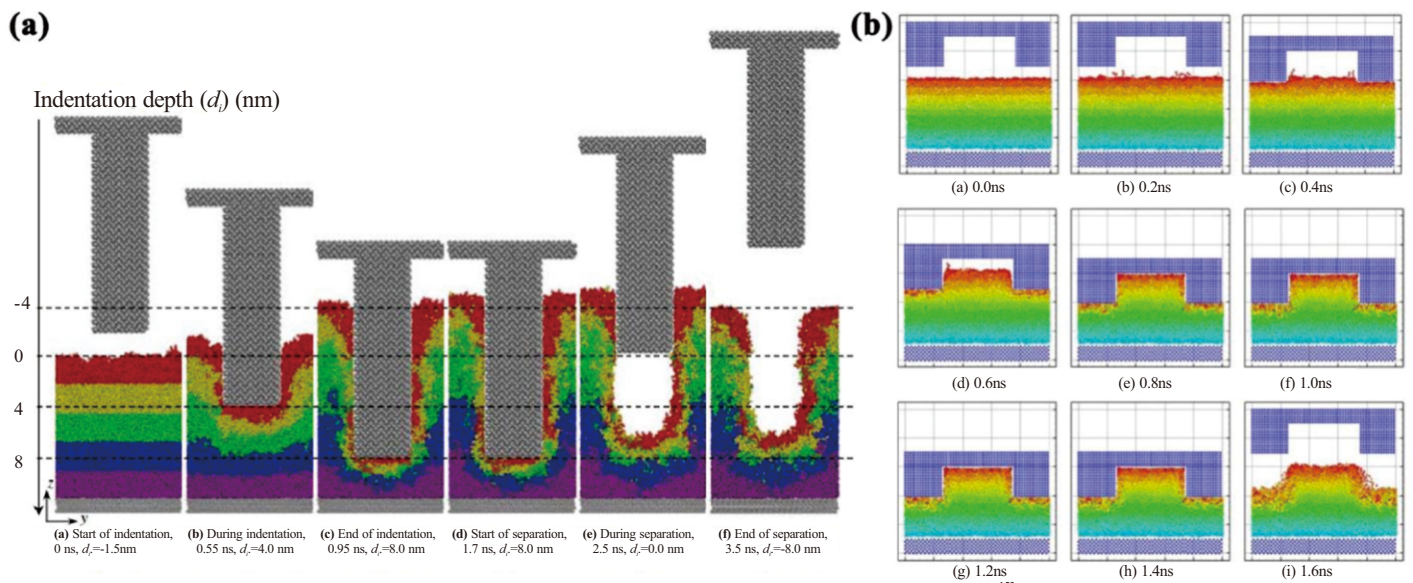


Fig. 10 MD simulation results of the hot embossing processes using (a) male (Reproduced with permission<sup>155</sup>) and (b) female molds (Reproduced with permission<sup>158</sup>).

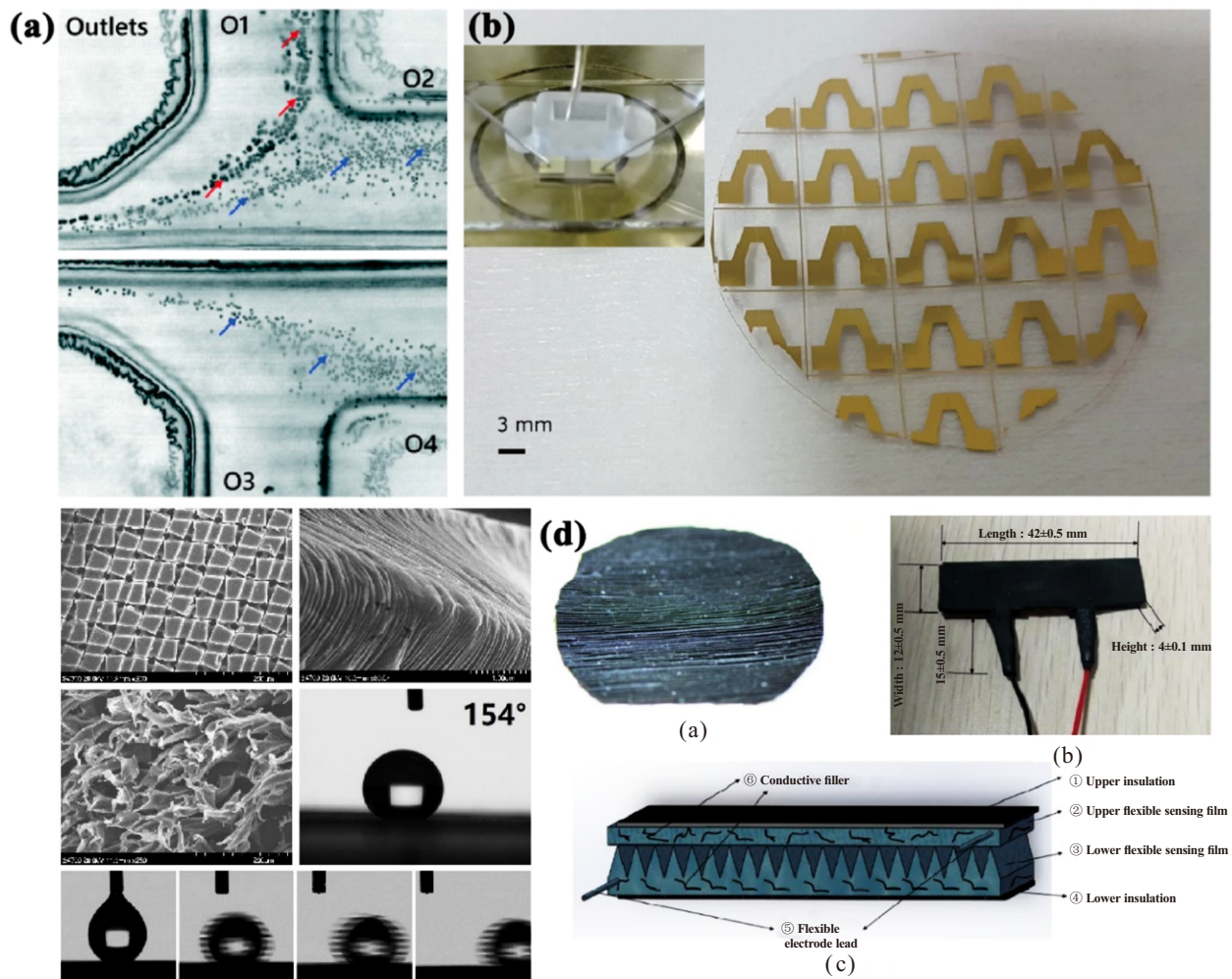


Fig. 11 (a) Successful sorting of 15  $\mu$ m (red arrows) and 10  $\mu$ m (blue arrows) diameter microparticles at the outlets of PMMA microfluidics (Reproduced with permission<sup>163</sup>); (b) The G-FET device fabricated using the method of single-layer graphene transfer based on the hot embossing on COC substrate (Reproduced with permission<sup>184</sup>); (c) The biomimetic hierarchical structures fabricated by the hot embossing and the derived superhydrophobic performance; (d) The sample image and schematic diagram of the polymeric flexible piezoresistive sensor.

patterned structures are conducive to the achievement of high-quality structure replications. In general, the mold fabrication methods can be classified into two major categories: direct structuring methods and lithography (LIGA)-based methods. All of these methods are widely used in mold fabrication for the hot embossing method and are even used in some other manufacturing methods because they have the ability of structural patterning on the micro- and nano-scales. Each method has its own characteristics and advantages and is therefore suitable for different applications.

Direct structuring methods are a class of one-step forming methods, while the LIGA-based methods are stepwise structuring methods. Direct structuring methods consist of micro-machining (e.g. single point diamond turning), laser structuring (e.g. femtosecond laser), electroplating, electric discharge machining (EDM), among others.<sup>159-163</sup> These methods have the advantages of ease of large-scale fabrication, easy operation, and suitable for the fabrication of metal molds. The LIGA-based methods consist of UV LIGA, soft-LIGA, laser LIGA, E-beam LIGA, and X-ray LIGA.<sup>164-167</sup> The processing procedure for the most widely used LIGA-based method, the UV LIGA method, is the following: First, a layer of conductive material is coated onto the substrate surface. Second, a layer of a UV sensitive polymer material is deposited onto the conductive material layer. Then, an irradiation step is performed under the mask with a pattern designed to complete the curing process of the flowable UV sensitive polymer material. After the dissolution of the chemically modified material, the polymeric mold with the desired structure can be obtained. Besides the methods of mold

fabrication, the mold material is also an important factor in determining the product quality of the hot embossing process. Metal, silicon, quartz, and polymers are the most commonly used mold materials for the hot embossing method in polymer processing. Among all the mold materials, metal molds present a relatively long longest service life and manufacturing cost (especially for nano-structured metal molds). Moreover, the mold fabrication method should be selected reasonably according to the mold material. Generally, metal molds, silicone molds, and other inorganic material molds are fabricated by direct structuring methods, while polymeric molds are typically fabricated by LIGA-based methods for the preparation of prototype products. A brief comparison between the structure sizes, structure geometries, and mold materials of different mold fabrication methods is listed in Table 2 below.

## 6. Applications of Polymer-Based Devices Prepared by Hot Embossing

Polymer-based devices prepared by hot embossing play an important role in many fields because of the designed micro/nano-structures that provide various unique properties. The application of hot embossing products as optical components, drug delivery devices, MEMS devices, antireflective films, and superhydrophobic/superhydrophilic surfaces have already been widely researched and reported by the researchers internationally.<sup>179-182</sup> Liu *et al.*<sup>183</sup> reported a continuous fabrication process for antireflective structures on the surface of 60  $\mu\text{m}$  thick polyethylene terephthalate (PET) films using an R2R hot embossing technique for the production of solar cells. Self-assembled, nanosphere-patterned nickel-

**Table 2** A brief comparison between different mold fabrication methods.

Structure size	Structure geometry	Mold material	Mold fabrication method	Ref.
20 $\mu\text{m}$ depth, 27 $\mu\text{m}$ spacing	Micro V -grooves and micro pyramids	Nickel alloy and mold steel	Elliptical vibration cutting	[168]
200 $\mu\text{m}$	Micro-pyramids	Nickel silver N37	Dimond micro -chiseling	[169]
40, 100, 150 $\mu\text{m}$ depths, 200 $\mu\text{m}$ -1 mm widths	Micro-channels	Polymethylmethacrylate	Micro-milling	[170]
14 $\mu\text{m}$ diameter, 6.8 $\mu\text{m}$ height	Micro-holes	Polyimide	UV LIGA	[171]
10 $\mu\text{m}$ diameter, 15 $\mu\text{m}$ height	Micro-pillars	Polydimethylsiloxane	Soft LIGA	[172]
0.6-0.7 $\mu\text{m}$ period, ~0.2 $\mu\text{m}$ height	Antireflective structure	Stainle ss steel	Femtosecond laser	[173]
2 $\mu\text{m}$ width, 1.5 $\mu\text{m}$ height	Micro-channels	Silicon wafer (0.5 mm thickness)	Reactive ion etching	[124]
360 $\mu\text{m}$ diameter, ~2.5 $\mu\text{m}$ height	Lenslets	Silicon wafer (5 mm thickness)	Single point diamond machining	[124]
61.5 $\mu\text{m}$ width, ~50 $\mu\text{m}$ depth	Micro-channels	Aluminum	Micro-EDM	[174]
20 $\mu\text{m}$ diameter	Micro-spikes	NAK80 metal mold	Laser ablation	[175]
0.7, 1.0, 1.5 pitches	Antireflective structure	Silicon	E-beam LIGA	[176]
44.5-280 $\mu\text{m}$ depth	Micro V -grooves	Polymethylmethacrylate	CO <sub>2</sub> laser LIGA	[177]
35 $\mu\text{m}$ height	Micro-channels	Copper	Electroplating	[178]

cobalt membranes with different feature sizes (471, 628, and 1200 nm) were used as the mold during the hot embossing process, and the optimal processing parameters were also systematically investigated for better forming results. The results showed that the feature heights of the antireflective nanostructures increased with the increase of the embossing pressure and the mold temperature, while decreased with the speed of the embossing roller. Moreover, PET films with antireflective structures could significantly reduce the reflectance and enhance the conversion efficiency of solar cells. The films with the 471 nm feature size presented an energy conversion efficiency of 16%, while those of films with 628, 1200 nm feature sizes and no structure were 15.3%, 13.4%, and 12.8%, respectively. Papautsky and co-workers<sup>113</sup> presented a novel inertial micro-fluidic chip with a low aspect ratio that was fabricated by a high-throughput R2R hot embossing process with the goal of size-based sorting of cells and microbeads. Fig. 11a shows the sorting result of 15  $\mu\text{m}$  (red arrows) and 10  $\mu\text{m}$  (blue arrows) diameter micro-particles using the obtained micro-fluidic chip. The researchers demonstrated that a sorting efficiency of  $>97\%$  was available for the continuous sorting of a mixture of 15  $\mu\text{m}$  and 10  $\mu\text{m}$  diameter micro-particles using this low cost and disposable PMMA inertial microfluidic chip. Balesio's group<sup>184</sup> proposed a novel, single-layer graphene transfer method based on the hot embossing process. Graphene field-effect transistors (G-FET) devices with flexible electrolyte gates were fabricated on the surface of a cyclic olefin copolymer (COC) substrate and then were tested systematically (as shown in Fig. 11b). The G-FET devices showed valid performances and maintained the same characteristics when bent with a relatively low curvature radius of 8 mm. The researchers further indicated that the G-FET devices on the flexible COC substrates had great potential in portable, highly-sensitive biomedical sensors.

Our research group has also done a lot of research on polymer-based devices prepared by hot embossing. For example, a new kind of aluminum-PP (metal-polymer) composite heat exchanger with V-shape microgrooves was proposed to meet the increasing requirement for efficient thermal dissipation within a confined space.<sup>185,186</sup> The V-shape microgrooves with a feature height of 25  $\mu\text{m}$  were fabricated via the aforementioned IHES method on PP substrate. The results of thermal dissipation experiments proved that the metal-polymer composite heat exchanger had almost the same thermal dissipation performance as a commercial aluminum heat exchanger, while the spatial volume of the former was only one-fifth of the latter. We had also fabricated polymeric superhydrophobic surfaces via the hot embossing technology.<sup>12</sup> Biomimetic hierarchical roughness was obtained without any chemical treatment using stainless steel meshes as the molds. The influences of processing parameters (e.g. mold temperature, pressure, and mesh number) were systematically investigated to achieve the best hydrophobic effect. The largest water contact angle of  $154^\circ$  and the lowest water sliding angle of  $\sim 1^\circ$  were achieved simultaneously under the joint action of hierarchical micro-platforms, micro-fibers, and the oriented array of nanowrinkles structured on them (as shown in Fig. 11c). Fig. 11d presented the sample image and schematic diagram of a polymeric flexible piezoresistive sensor that was prepared via the hot embossing technique.<sup>67,187,188</sup> A polydimethylsiloxane (PDMS)/short carbon fiber (SCF) composite was selected as the basic material of this piezoresistive sensor. The method of spatial confining forced network assembly (SCFNA), which was a derivative technology of the hot embossing method, was applied for the preparation of the micro-structured pressure sensing components. The sensor showed a stable sensing performance and a relatively narrow accuracy fluctuation range within  $\pm 7\%$  for polymeric sensors under both dynamic and static loads. Besides, we had also applied the hot embossing method for the

fabrication of a micro-needle array on PMMA substrates.<sup>189,190</sup> The edge effect in the hot embossing method on the formation of micro-needles was investigated using both numerical and experimental methods. An optimized mold design of the convex flow barrier was further proposed to improve the structure uniformity and replication efficiency of the products fabricated by the hot embossing method.

## 7. Conclusion and Outlook

Micro/nano-manufacturing is at the frontier of science and technology with the rapid development speed for interdisciplinary applications, such as micro-electromechanical systems (MEMS), superhydrophobic/superhydrophilic surfaces, antireflection films, and other functional polymer-based devices. Micro- and nano-structured devices are important components of many newly developed systems, and the product quality, fabricating efficiency, and cost of the manufacturing methods would directly affect their application and developing in industry. In the field of manufacturing, polymer material present advantages such as a low cost, high machinability, good corrosion resistance, and biocompatibility. Thus, the development and fabrication of polymer-based micro-/nano-structured devices have already become one of the research hotspots and vital developing aspects of micro/nano-manufacturing technologies.

The hot embossing method, as one of the most widely used polymer micro/nano-manufacturing technologies, has already experienced a rapid development period for more than 20 years. There are three basic implementations of the hot embossing method, including plate-to-plate (P2P), roll-to-plate (R2P), and roll-to-roll (R2R) hot embossing. New and improved methods are successively being developed and applied in laboratories and industries. Although researchers around the world have already proposed a series of modified hot embossing methods, there are still significant improvements in processing efficiency and accuracy that need to be for the complete commercial viability of the process. Several future trends of hot embossing in polymer processing are listed below:

(1) In the long run, the processing efficiency is the most influential factor in determining the success of commercialization. Therefore, R2R hot embossing presents a greater potential compared to P2P and R2P hot embossing, as the R2R method is a truly continuous fabrication method with high efficiency and high accuracy. The application and development of a complete set of technology and equipment for the R2R type to achieve continuous large-scale nanostructure arrays on polymer substrates will become one of the most promising research directions. For many researchers, the goal is to achieve a system for the mass production of structured polymeric products with low costs and high efficiency.

(2) Higher processing accuracy of the hot embossing technology demands better control precision and adaptability of the manufacturing equipment. Higher machining precision of structured molds is also helpful for quality improvement of the polymeric products prepared by the hot embossing method. However, there are still many difficulties in the fabrication of high-precision molds, especially in the case of molds with nanoscale features. Thus, a future area of exploration for the hot embossing method is the additional development and improvement in mold fabrication processes.

(3) In-depth, fundamental, theoretical research on the hot embossing process, including the mold filling and demolding stages, is a crucial research direction for better understanding of polymer processing. For example, the influence of the size effect on polymer flow behavior and its consequent influences on the forming quality of polymer micro/nano-structured devices needs to be systematically investigated.

(4) The processing window analysis of the hot embossing

technology for different kinds of polymer materials is a potential future research direction in order to broaden the application range and raise the reliability of hot embossing methods. Not only for commonly used polymers (e.g. PP, PMMA, PET), but also for special engineered plastics and the polymer materials with special properties (e.g. shape-memory materials and gel materials).

(5) Last but not least, the integration of the hot micro/nano-embossing technology with other material processing technologies and the integration of micro/nano-structured polymeric products with other functional devices are also future research directions to broaden the potential applications and increase the added value of the hot embossing technology.

## Nomenclature

$T_g$  – Glass transition temperature;  
 $T_m$  – Melting temperature;  
 $T_f$  – Viscous flow temperature;  
 $T_R$  – Room temperature;  
 $T_E$  – Embossing temperature;  
 $T_D$  – Demolding temperature;  
 $P_E$  – Embossing pressure;  
 $T_{mold}$  – Mold temperature;  
 P2P – Plate-to-plate;  
 R2P – Roll-to-plate;  
 R2R – Roll-to-roll;  
 RTR – Rapid thermal response;  
 PMMA – Polymethylmethacrylate;  
 PP – Polypropylene;  
 IHES – Isothermal hot embossing in the solid-like state;  
 PET – Polyethylene terephthalate;  
 PEEK – Polyether ether ketone;  
 FEM – Finite element method;  
 MD – molecular dynamics;  
 PE – Polyethylene;  
 LIGA – Lithography;  
 EDM – Electric discharge machining;  
 G-FET – Graphene field-effect transistors;  
 COC – Cyclic olefin copolymer;  
 PDMS – Polydimethylsiloxane;  
 SCF – Short carbon fiber;  
 SCFNA – Spatial confining forced network assembly;  
 MEMS – Micro-electromechanical systems;  
 $\Phi_{bond}$  – Potential energy expressions for translation of the polymer chains;  
 $\Phi_{angle}$  – Potential energy expressions for rotation of the polymer chains;  
 $\Phi_{torsion}$  – Potential energy expressions for torsion of the polymer chains;  
 $l_{ij}$  – Bond length;  
 $l_0$  – Equilibrium bond length;  
 $K_{bond}$ ,  $K_{angle}$ , and  $a_m$  – Energy constants;  
 $\theta_{ijk}$  – Bending angle;  
 $\theta_0$  – Equilibrium bending angle;  
 $\theta_{jkl}$  – Twist angle;

## Acknowledgments

The authors gratefully thank the financial support of National Natural Science Foundation of China (Nos. 51673020 and 51173015), the Fundamental Research Funds for Central Universities (No. JD1910), and the Talents Introduction Project in Beijing University of Chemical Technology (No. buctrc201909).

## References

- W. S. Chu, C. S. Kim, H. T. Lee, J. O. Choi, J. I. Park, J. H. Song, K. H. Jang and S. H. Ahn, *Int. J. Pr. Eng. Man-GT*, 2014, 1, 75-92
- E. B. Hrousseau, S. S. Dimov and D. T. Pham, *Int. J. Adv. Manuf.*, 2009, 47, 161-180
- Y. Qin, A. Brockett, Y. Ma, A. Razali, J. Zhao, C. Harrison, W. Pan, X. Dai and D. Loziak, *Int. J. Adv. Manuf.*, 2009, 47, 821-837
- C. Zhang, D. A. McAdams and J. C. Grunlan, *Adv. Mater.*, 2016, 28, 8566-8566
- S. Gao and H. Huang, *Front. Mech. Eng.*, 2017, 12, 18-32
- K. S. Ramadan, D. Sameoto and S. Evoy, *Sm.Ma.S.*, 2014, 23, 033001
- M. Irimia-Vladu, *Chem. Soc. Rev.*, 2014, 43, 588-610
- X. Wang, M. Jiang, Z. Zhou, J. Gou and D. Hui, *Compos. Part B-Eng.*, 2017, 110, 442-458
- J. Chen, X. Huang, B. Sun and P. Jiang, *ACS Nano*, 2018, 13, 337-345
- J. Sun, J. Shen, S. Chen, M. Cooper, H. Fu, D. Wu and Z. Yang, *Polymers*, 2018, 10, 505
- D. Gong, J. Long, P. Fan, D. Jiang, H. Zhang and M. Zhong, *ApSS*, 2015, 331, 437-443
- J. Sun, H. Li, Y. Huang, X. Zheng, Y. Liu, J. Zhuang and D. Wu, *ACS Omega*, 2019, 4, 2750-2757
- C. Weng, F. Wang, M. Zhou, D. Yang and B. Jiang, *ApSS*, 2018, 436, 224-233
- C. K. Söz, E. Yilgör and I. Yilgör, *Poly*, 2016, 99, 580-593
- Z. Xiong, H. Lin, Y. Zhong, Y. Qin, T. Li and F. Liu, *J. Mater. Chem. A*, 2017, 5, 6538-6545
- R. Ou, J. Wei, L. Jiang, G. P. Simon and H. Wang, *Environ. Sci. Technol.*, 2016, 50, 906-914
- F. Noorisafa, A. Razmjou, N. Emami, Z. X. Low, A. H. Korayem and A. A. Kajani, *J. Exp. Nanosci.*, 2016, 11, 1087-1109
- J. Sun, X. Wang, J. Wu, C. Jiang, J. Shen, M. A. Cooper, X. Zheng, Y. Liu, Z. Yang and D. Wu, *Sci. Rep.*, 2018, 8
- L. Sainiemi, V. Jokinen, A. Shah, M. Shpak, S. Aura, P. Suvanto and S. Franssila, *Adv. Mater.*, 2011, 23, 122-126
- G. Li, J. Li, C. Zhang, Y. Hu, X. Li, J. Chu, W. Huang and D. Wu, *ACS Appl. Mater. Int.*, 2014, 7, 383-390
- C. H. Chien and Z. P. Chen, *MSF*, 2006, 505-507, 211-216
- S. W. Kim, H. G. Kim, S. E. Lee, H. Lee and H. C. Lee, *Nanosci. Nanotech. Let.*, 2016, 8, 13-20
- L. Zhou, X. Dong, Y. Zhou, W. Su, X. Chen, Y. Zhu and S. Shen, *ACS Appl. Mater. Int.*, 2015, 7, 26989-26998
- K. Maghsoudi, R. Jafari, G. Momen and M. Farzaneh, *Mater. Today Commun.*, 2017, 13, 126-143
- M. Shi, D. Wu, Y. Liu, Y. Huang, J. Sun and C. Leng, *ApCM*, 2019, 26, 1139-1150
- X. Sánchez-Sánchez, M. Hernández-Avila, L. E. Elizalde, O. Martínez, I. Ferrer and A. Elías-Zuñiga, *Mater. Design*, 2017, 132, 1-12
- M. Zhou, X. Xiong, B. Jiang and C. Weng, *ApSS*, 2018, 427, 854-860
- D. C. Duffy, J. C. McDonald, O. J. A. Schueller and G. M. Whitesides, *AnaCh*, 1998, 70, 4974-4984
- M. Soleymaniha and J. R. Felts, *IJHMT*, 2016, 101, 166-174
- T. D. Brown, P. D. Dalton and D. W. Huttmacher, *Prog. Polym. Sci.*, 2016, 56, 116-166
- J. K. Y. Lee, N. Chen, S. Peng, L. Li, L. Tian, N. Thakor and S. Ramakrishna, *Prog. Polym. Sci.*, 2018, 86, 40-84
- T. Jiang, E. J. Carbone, K. W. H. Lo and C. T. Laurencin, *Prog. Polym. Sci.*, 2015, 46, 1-24
- S. Hong, D. Sycks, H. F. Chan, S. Lin, G. P. Lopez, F. Guilak, K. W. Leong and X. Zhao, *Adv. Mater.*, 2015, 27, 4035-4040
- M. Zarek, M. Layani, I. Cooperstein, E. Sachyani, D. Cohn and S. Magdassi, *Adv. Mater.*, 2016, 28, 4449-4454
- R. J. Mondschein, A. Kanitkar, C. B. Williams, S. S. Verbridge and T. E. Long, *Biomaterials*, 2017, 140, 170-188
- L. Peng, Y. Deng, P. Yi and X. Lai, *JMiMi*, 2014, 24, 013001
- J. Sun, D. Wu, Y. Liu, L. Dai and C. Jiang, *Adv. Polym. Tech.*, 2018, 37, 1581-1591
- S. Falah Toosi, S. Moradi, M. Ebrahimi and S. G. Hatzikiriakos, *ApSS*, 2016,

- 378, 426-434
39. S. Schauer, T. Meier, M. Reinhard, M. Röhrig, M. Schneider, M. Heilig, A. Kolew, M. Worgull and H. Hölscher, *ACS Appl. Mater. Int.*, 2016, 8, 9423-9430
40. A. Rank, T. Kunze, T. Hoffmann and A. F. Lasagni, *Adv. Eng. Mater.*, 2016, 18, 1280-1288
41. M. T. Gale, *MiEng*, 1997, 34, 321-339
42. H. Mizuno, O. Sugihara, T. Kaino, N. Okamoto and M. Hosino, *OptL*, 2003, 28, 2378
43. M. Yonemura, A. Kawasaki, S. Kato, M. Kagami and Y. Inui, *OptL*, 2005, 30, 2206
44. R. Ahmed, A. K. Yetisen and H. Butt, *ACS Nano*, 2017, 11, 3155-3165
45. H. Jung and K.-H. Jeong, *ACS Appl. Mater. Int.*, 2015, 7, 2160-2165
46. S. Moore, J. Gomez, D. Lek, B. H. You, N. Kim and I. H. Song, *MiEng*, 2016, 162, 57-62
47. P. D. Cunningham, J. B. Souza, I. Fedin, C. She, B. Lee and D. V. Talapin, *ACS Nano*, 2016, 10, 5769-5781
48. C. H. Wu and C. H. Lu, *JMiMi*, 2008, 18, 035006
49. C. W. Fuller, S. Kumar, M. Porel, M. Chien, A. Bibillo, P. B. Stranges, M. Dorwart, C. Tao, Z. Li, W. Guo, S. Shi, D. Korenblum, A. Trans, A. Aguirre, E. Liu, E. T. Harada, J. Pollard, A. Bhat, C. Cech, A. Yang, C. Arnold, M. Palla, J. Hovis, R. Chen, I. Morozova, S. Kalachikov, J. J. Russo, J. J. Kasianowicz, R. Davis, S. Roevers, G. M. Church and J. Ju, *P. Acad. Sci.*, 2016, 113, 5233-5238
50. J. Li and E. C. Lee, *Biosensors Bioelectron.*, 2015, 71, 414-419
51. H. Doi, T. Takahara, T. Minamoto, S. Matsushashi, K. Uchii and H. Yamanaka, *Environ. Sci. Technol.*, 2015, 49, 5601-5608
52. F. Hao, Y. Li, J. Zhu, J. Sun, B. Marshall, R. J. Lee, L. Teng, Z. Yang and J. Xie, *Curr. Med. Chem.*, 2019, 26, 2264-2284
53. D. Xia, J. Yan and S. Hou, *Small*, 2012, 8, 2787-2801
54. M. I. Mohammed and M. P. Y. Desmulliez, *Lab Chip*, 2011, 11, 569-595
55. J. Sun, S. Kormakov, Y. Liu, Y. Huang, D. Wu and Z. Yang, *Molecules*, 2018, 23, 1704
56. J. M. Lee, M. Zhang and W. Y. Yeong, *Microfluid. Nanofluid.*, 2016, 20
57. C. W. Tsao, *Micromachines*, 2016, 7, 225
58. C. Delaney, P. McCluskey, S. Coleman, J. Whyte, N. Kent and D. Diamond, *LChip*, 2017, 17, 2013-2021
59. X. Hou, Y. S. Zhang, G. T.-d. Santiago, M. M. Alvarez, J. Ribas, S. J. Jonas, P. S. Weiss, A. M. Andrews, J. Aizenberg and A. Khademhosseini, *Nat. Rev. Mater.*, 2017, 2
60. H. Wu, J. Zhu, Y. Huang, D. Wu and J. Sun, *Molecules*, 2018, 23, 2347
61. A. S. Kastania, K. Tsougeni, G. Papadakis, E. Gizeli, G. Kokkoris, A. Tserepi and E. Gogolides, *Anal. Chim. Acta*, 2016, 942, 58-67
62. C. Y. Lee and L. M. Fu, *Sensors Actuators B: Chem.*, 2018, 259, 677-702
63. F. J. Lara, D. Airado-Rodríguez, D. Moreno-González, J. F. Huertas-Pérez and A. M. García-Campaña, *Anal. Chim. Acta*, 2016, 913, 22-40
64. X. Chen and L. Zhang, *Sensors Actuators B: Chem.*, 2018, 254, 648-659
65. M. Heckele and W. K. Schomburg, *JMiMi*, 2004, 14, R1-R14
66. M. Vaezi, H. Seitz and S. Yang, *Int. J. Adv. Manuf.*, 2012, 67, 1721-1754
67. H. Liu, R. Jian, H. Chen, X. Tian, C. Sun, J. Zhu, Z. Yang, J. Sun and C. Wang, *Nanomaterials*, 2019, 9, 950
68. Y. Huang, S. Kormakov, X. He, X. Gao, X. Zheng, Y. Liu, J. Sun and D. Wu, *Polymers*, 2019, 11, 187
69. X. He, Y. Huang, C. Wan, X. Zheng, S. Kormakov, X. Gao, J. Sun, X. Zheng and D. Wu, *Composites Sci. Technol.*, 2019, 172, 163-171
70. Y. Chen, *Appl. Phys. A*, 2015, 121, 451-465
71. J. T. Wu, W. Y. Chang and S. Y. Yang, *JMiMi*, 2010, 20, 075023
72. W. Zou, J. Sackmann, A. Striegel, M. Worgull and W. K. Schomburg, *Microsyst. Technol.*, 2019, 25, 4185-4195
73. C. C. Kuo and T.-S. Chiang, *Int. J. Adv. Manuf.*, 2016, 91, 1321-1326
74. R. Bartolini, W. Hannan, D. Karlsons and M. Lurie, *ApOpt*, 1970, 9, 2283
75. R. Ulrich, H. P. Weber, E. A. Chandross, W. J. Tomlinson and E. A. Franke, *ApPhL*, 1972, 20, 213-215
76. S. Y. Chou, P. R. Krauss and P. J. Renstrom, *ApPhL*, 1995, 67, 3114-3116
77. C. C. Cheng, S. Y. Yang and D. Lee, *Sensors*, 2014, 14, 19493-19506
78. M. Worgull, *Journal of Micro/Nanolithography, MEMS, and MOEMS*, 2006, 5, 011005
79. A. Kolew, D. Münch, K. Sikora and M. Worgull, *Microsyst. Technol.*, 2010, 17, 609-618
80. C. Liu, J. M. Li, J. S. Liu and L. D. Wang, *MiEng*, 2010, 87, 200-207
81. A. Kolew, M. Heilig, M. Schneider, D. Münch, R. Ezzat, N. Schneider and M. Worgull, *Microsystem Technologies*, 2013, 20, 1967-1973
82. N. Zhang, A. Srivastava, B. Kirwan, R. Byrne, F. Fang, D. J. Browne and M. D. Gilchrist, *JMiMi*, 2015, 25, 095005
83. S. H. Hong, J. Hwang and H. Lee, *Nanot*, 2009, 20, 385303
84. Z. Yin, E. Cheng and H. Zou, *Lab Chip*, 2014, 14, 1614-1621
85. A. Habermehl, P. Brenner, R. Huber, A. Mertens, F. Winkler, L. Hahn, M. Guttman, C. Eschenbaum and U. Lemmer, *Adv. Eng. Mater.*, 2019, 21, 1900110
86. X. Song, X. C. Shan, S. L. Chow, X. Y. Deng and W. S. Teo, *Microsyst. Technol.*, 2014, 21, 1729-1738
87. L. Dhakar, S. Gudla, X. Shan, Z. Wang, F. E. H. Tay, C. H. Heng and C. Lee, *Sci. Rep.*, 2016, 6
88. S. J. Choi and S. K. Kim, *J. Mech. Sci. Technol.*, 2011, 25, 117-124
89. S. K. Kim, S. J. Choi, K. H. Lee, D. J. Kim and Y. E. Yoo, *Polym. Eng. Sci.*, 2010, 50, 1377-1381
90. L. Xie, G. Ziegmann, M. Hlavac and R. Wittmer, *Microsyst. Technol.*, 2009, 15, 1031-1037
91. N. Zhang, D. J. Browne and M. D. Gilchrist, *Int. J. Eng. Technol.*, 2013, 198-201
92. J. Rajabi, N. Muhamad and A. B. Sulong, *Microsyst. Technol.*, 2012, 18, 1941-1961
93. E. Zanchetta, E. Guidi, G. Della Giustina, M. Sorgato, M. Krampera, G. Bassi, R. Di Liddo, G. Lucchetta, M. T. Conconi and G. Brusatin, *ACS Appl. Mater. Int.*, 2015, 7, 7273-7281
94. C. Yang, X. H. Yin and G. M. Cheng, *JMiMi*, 2013, 23, 093001
95. N. Zhang, J. S. Chu, C. J. Byrne, D. J. Browne and M. D. Gilchrist, *JMiMi*, 2012, 22, 065019
96. D. Annicchiarico and J. R. Alcock, *MMP*, 2014, 29, 662-682
97. M. W. Fu and W. L. Chan, *Int. J. Adv. Manuf.*, 2012, 67, 2411-2437
98. T. Nathan-Walleiser, I.-M. Lazar, M. Fabritius, F. J. Tölle, Q. Xia, B. Bruchmann, S. S. Venkataraman, M. G. Schwab and R. Mülhaupt, *Adv. Funct. Mater.*, 2014, 24, 4706-4716
99. E. S. Bochmann, D. Neumann, A. Gryczke and K. G. Wagner, *Eur. J. Pharm. Biopharm.*, 2016, 107, 40-48
100. W. L. Chan, M. W. Fu and J. Lu, *Mater. Design*, 2011, 32, 525-534
101. D. Yao and B. Kim, *JMiMi*, 2002, 12, 604-610
102. N. T. Intawong and N. Sombatsompop, *Polym. Eng. Sci.*, 2004, 44, 2298-2307
103. Y. K. Dai, C. X. Zhou and W. Yu, *Plastics, Rubber Compos.*, 2013, 36, 141-148
104. M. W. Williams, D. Kothe, D. Korzekwa and P. Tubesing, 2002, 751-759
105. C. S. Chen, S. C. Chen, W. L. Liaw and R. D. Chien, *Eur. Polym. J.*, 2008, 44, 1891-1898
106. S. Granick, Y. Zhu and H. Lee, *Nat. Mater.*, 2003, 2, 221-227
107. X. Liang, Y. S. Jung, S. Wu, A. Ismach, D. L. Olynick, S. Cabrini and J. Bokor, *Nano Lett.*, 2010, 10, 2454-2460
108. S. W. Lee, K. S. Lee, J. Ahn, J. J. Lee, M. G. Kim and Y. B. Shin, *ACS Nano*, 2011, 5, 897-904
109. J. C. Yang and C. C. Huang, *Mic. Nano Lett.*, 2012, 7, 244
110. J. J. Dumond and H. Yee Low, *J. Vac. Sci. Technol. B*, 2012, 30, 010801
111. T. Velten, F. Bauerfeld, H. Schuck, S. Scherbaum, C. Landesberger and K. Bock, *Microsyst. Technol.*, 2010, 17, 619-627
112. V. Lang, A. Rank and A. F. Lasagni, *Adv. Eng. Mater.*, 2017, 19, 1700126
113. X. Wang, C. Liedert, R. Liedert and I. Papautsky, *LChip*, 2016, 16, 1821-1830
114. Z. W. Zhong, H. H. Ng, S. H. Chen and X. C. Shan, *Microsyst. Technol.*, 2017, 24, 1443-1452
115. Y. Vladimirov, M. Colburn, S. C. Johnson, M. D. Stewart, S. Damle, T. C. Bailey, B. Choi, M. Wedlake, T. B. Michaelson, S. V. Sreenivasan, J. G. Ekerdt and C. G. Willson, 1999, 3676, 379
116. X. C. Shan, T. Ikehara, Y. Murakoshi and R. Maeda, *Sensors Actuat. A-Phys.*, 2005, 119, 433-440
117. S. W. Youn, M. Ogiwara, H. Goto, M. Takahashi and R. Maeda, *J. Mater. Process. Technol.*, 2008, 202, 76-85
118. Y. Deng, P. Yi, L. Peng, X. Lai and Z. Lin, *JMiMi*, 2014, 24, 045023

119. D. Wu, J. Sun, Y. Liu, Z. Yang, H. Xu, X. Zheng and P. Gou, *Polym. Eng. Sci.*, 2017, 57, 268-274
120. S. Jingyao, W. Daming, L. Ying, Y. Zhenzhou and G. Pengsheng, *Polym. Eng. Sci.*, 2018, 58, 952-960
121. T. E. Kimerling, W. Liu, B. H. Kim and D. Yao, *Microsyst. Technol.*, 2006, 12, 730-735
122. H. Mekar, O. Nakamura, O. Maruyama, R. Maeda and T. Hattori, *Microsyst. Technol.*, 2006, 13, 385-391
123. S. J. Liu, K. Y. Lin and M. K. Li, *Int. Polym. Proc.*, 2008, 23, 323-330
124. P. Xie, P. He, Y. C. Yen, K. J. Kwak, D. Gallego-Perez, L. Chang, W. C. Liao, A. Yi and L. J. Lee, *SuCT*, 2014, 258, 174-180
125. Y. He, J. Z. Fu and Z. C. Chen, *JMiMi*, 2007, 17, 2420-2425
126. Y. He, W. Wu, T. Zhang and J. Fu, *RSC Adv.*, 2015, 5, 39138-39144
127. N. Wiriyakun, D. Nacapricha and R. Chantiwas, *Talanta*, 2016, 161, 574-582
128. R. K. R. Thanumoorthy, B. H. Kim and D. Yao, *Polym. Eng. Sci.*, 2014, 54, 1100-1112
129. S. Y. Chou, *J. Vac. Sci. Technol. B*, 1997, 15, 2897
130. L. J. Guo, *J. Phys. D: Appl. Phys.*, 2004, 37, R123-R141
131. D. Y. Khang and H. H. Lee, *ApPhL*, 2000, 76, 870-872
132. M. C. Traub, W. Longsine and V. N. Truskett, *Annu. Rev. Chem. Biomol.*, 2016, 7, 583-604
133. H. Schiff, *Appl. Phys. A*, 2015, 121, 415-435
134. Z. Yu and S. Y. Chou, *Nano Lett.*, 2004, 4, 341-344
135. D. Mathiesen, D. Vogtmann and R. B. Dupaix, *Mech. Mater.*, 2014, 71, 74-84
136. G. Cheng and T. Barriere, *Int. J. Adv. Manuf.*, 2019, 103, 549-565
137. Y. Hirai, T. Konishi, T. Yoshikawa and S. Yoshida, *J. Vacu. Sci. Technol. Bs*, 2004, 22, 3288
138. M. R. Sonne, K. Smistrup, M. Hannibal, J. Thorborg, J. Nørregaard and J. H. Hattel, *J. Mater. Process. Technol.*, 2015, 216, 418-429
139. E. Cheng, Z. Yin, H. Zou and P. Jurčiček, *JMiMi*, 2014, 24, 015004
140. W. B. Young, *MiEng*, 2005, 77, 405-411
141. Z. Song, B. H. You, J. Lee and S. Park, *Microsyst. Technol.*, 2008, 14, 1593-1597
142. M. Sahli, B. Mamen, H. Ou, J. C. Gelin, T. Barrière and M. Assoul, *Int. J. Adv. Manuf.*, 2018, 99, 1141-1154
143. J. Xu, L. Shi, C. Wang, D. Shan and B. Guo, *J. Mater. Process. Technol.*, 2015, 225, 375-384
144. Z. Yin, E. Cheng, H. Zou and P. Jurčiček, *Polym. Eng. Sci.*, 2014, 54, 2398-2406
145. S. Lan, H. J. Lee, S.-H. Lee, J. Ni, X. Lai, H. W. Lee, J. H. Song and M. G. Lee, *Mater. Design*, 2009, 30, 3879-3884
146. X. Zhang, G. Fang, T. Jiang, N. Zhao, J. Li, B. Dun and Q. Li, *Int. J. Precis. Eng. Manuf.*, 2015, 16, 2339-2346
147. T. Zhang, Y. He and J. Z. Fu, *Appl. Mech. Mater.*, 2011, 80-81, 339-345
148. D. Yao, V. L. Virupaksha and B. Kim, *Polym. Eng. Sci.*, 2005, 45, 652-660
149. J. S. Jha and S. S. Joshi, *Int. J. Precis. Eng. Manuf.*, 2012, 13, 2215-2224
150. S. Yang, S. Yu and M. Cho, *ApSS*, 2014, 301, 189-198
151. J. H. Kang, K. S. Kim and K. W. Kim, *ApSS*, 2010, 257, 1562-1572
152. Y. S. Woo, J. K. Kim, D. E. Lee, K. Y. Suh and W. I. Lee, *ApPhL*, 2007, 91, 253111
153. J. H. Kang, K. S. Kim and K. W. Kim, *TriL*, 2007, 25, 93-102
154. M. Chandross and G. S. Grest, *Langmuir*, 2011, 28, 1049-1055
155. A. Taga, M. Yasuda, H. Kawata and Y. Hirai, *J. Vacu. Sci. Technol. B*, 2010, 28, C6M68-C66M71
156. R. F. Gibson, *Compos. Sci. Technol.*, 2014, 105, 51-65
157. C. Li and A. Strachan, *J. Polym. Sci., Part B: Polym. Phys.*, 2015, 53, 103-122
158. Y. S. Woo, D. E. Lee and W. I. Lee, *TriL*, 2009, 36, 209-222
159. A. Mir, X. Luo and J. Sun, *Wear*, 2016, 364-365, 233-243
160. B. Goel, S. Singh and R. V. Sarepaka, *MMP*, 2014, 30, 1018-1025
161. E. Fadeeva, V. K. Truong, M. Stiesch, B. N. Chichkov, R. J. Crawford, J. Wang and E. P. Ivanova, *Langmuir*, 2011, 27, 3012-3019
162. K. Hili, D. Fan, V. A. Guzenko and Y. Ekinici, *MiEng*, 2015, 141, 122-128
163. K. Essa, F. Modica, M. Imbaby, M. A. El-Sayed, A. ElShaer, K. Jiang and H. Hassanin, *Int. J. Adv. Manuf.*, 2016, 91, 445-452
164. L. Du, M. Zhao, A. Wang, S. Chen and W. Nie, *Microsyst. Technol.*, 2014, 21, 2025-2032
165. H. Hassanin, H. Ostadi and K. Jiang, *Int. J. Adv. Manuf.*, 2012, 67, 2293-2300
166. R. Phatthanakun, C. Yunphuttha, C. Pantong, C. Sriphung, N. Chomnawang and P. Viravathana, 2013, 1-5
167. M. S. Mahmood, Z. Celik-Butler and D. P. Butler, *Sensor. Actuat. A-Phys.*, 2017, 263, 530-541
168. G. D. Kim and B. G. Loh, *Int. J. Precis. Eng. Manuf.*, 2011, 12, 583-588
169. E. Brinksmeier, R. Gläbe and L. Schönemann, *Precis. Eng.*, 2012, 36, 650-657
170. M. Jang, Y. J. Kwon and N. Y. Lee, *RSC Adv.*, 2015, 5, 100905-100911
171. N. Kodihalli Shivaprakash, T. Ferraguto, A. Panwar, S. S. Banerjee, C. F. Barry and J. Mead, *ACS Omega*, 2019, 4, 12480-12488
172. V. N. Goral, Y. C. Hsieh, O. N. Petzold, R. A. Faris and P. K. Yuen, *JMiMi*, 2011, 21, 017002
173. T. F. Yao, P. H. Wu, T. M. Wu, C. W. Cheng and S. Y. Yang, *MiEng*, 2011, 88, 2908-2912
174. M. S. Huang, Y. C. Chiang, S. C. Lin, H. C. Cheng, C. F. Huang, Y. K. Shen and Y. Lin, *Polym. Adv. Technol.*, 2012, 23, 57-64
175. J. Noh, J. H. Lee, S. Y. Lee and S. Na, *JaJAP*, 2010, 49, 106503
176. J. Y. Chen and K. W. Sun, *Sol. Energy Mater. Sol. Cells*, 2010, 94, 629-633
177. C. K. Chung, Y. J. Syu, H. Y. Wang, C. C. Cheng, S. L. Lin and K. Z. Tu, *Microsyst. Technol.*, 2012, 19, 439-443
178. S. R. Nugen, P. J. Asiello and A. J. Baemmer, *Microsyst. Technol.*, 2008, 15, 477-483
179. J. Sun, Y. Zhao, Z. Yang, J. Shen, E. Cabrera, M. J. Lertola, W. Yang, D. Zhang, A. Benatar, J. M. Castro, D. Wu and L. J. Lee, *Nanot*, 2018, 29, 355304
180. D. Wu, X. Gao, J. Sun, D. Wu, Y. Liu, S. Kormakov, X. Zheng, L. Wu, Y. Huang and Z. Guo, *Compos. Part A-Appl. S.*, 2017, 102, 88-95
181. X. He, Y. Huang, Y. Liu, X. Zheng, S. Kormakov, J. Sun, J. Zhuang, X. Gao and D. Wu, *JMatS*, 2018, 53, 14299-14310
182. J. Sun, J. Zhuang, J. Shi, S. Kormakov, Y. Liu, Z. Yang and D. Wu, *JMatS*, 2019, 54, 8436-8449
183. S. J. Liu and W. A. Chen, *Opt. Laser Technol.*, 2013, 48, 226-234
184. A. Ballesio, M. Parmeggiani, A. Vema, F. Frascella, M. Cocuzza, C. F. Pirri and S. L. Marasso, *MiEng*, 2019, 209, 16-19
185. J. Sun, J. Zhuang, H. Jiang, Y. Huang, X. Zheng, Y. Liu and D. Wu, *Appl. Therm. Eng.*, 2017, 121, 492-500
186. J. Zhuang, W. Hu, Y. Fan, J. Sun, X. He, H. Xu, Y. Huang and D. Wu, *Microsyst. Technol.*, 2018, 25, 381-388
187. Z. Yang, H. Xu, Y. Huang, J. Sun, D. Wu, X. Gao and Y. Zhang, *Sensors*, 2019, 19, 1403
188. F. Su, Z. Zhao, Y. Liu, W. Si, C. Leng, Y. Du, J. Sun and D. Wu, *J. Polym. Eng.*, 2019, 39, 892-901
189. J. Zhuang, D. M. Wu, H. Xu, Y. Huang, Y. Liu and J. Y. Sun, *Int. Polym. Proc.*, 2019, 34, 231-238
190. X. He, J. Sun, J. Zhuang, H. Xu, Y. Liu and D. Wu, *Dose-Response*, 2019, 17, 155932581987858

**Publisher's Note** Engineered Science Publisher remains neutral with regard to jurisdictional claims in published maps and institutional affiliations.